

Soft x-ray tomohology

This article has been downloaded from IOPscience. Please scroll down to see the full text article.

2012 New J. Phys. 14 013022

(<http://iopscience.iop.org/1367-2630/14/1/013022>)

View [the table of contents for this issue](#), or go to the [journal homepage](#) for more

Download details:

IP Address: 134.94.122.141

The article was downloaded on 08/08/2013 at 14:51

Please note that [terms and conditions apply](#).

Soft x-ray tomoholography

**Erik Guehrs^{1,2,5}, Andreas M Stadler², Sam Flewett¹,
Stefanie Frömmel¹, Jan Geilhufe³, Bastian Pfau¹,
Torbjörn Rander¹, Stefan Schaffert¹, Georg Büldt^{2,4}
and Stefan Eisebitt^{1,3}**

¹ Institut für Optik und Atomare Physik, Technische Universität Berlin,
Hardenbergstrasse 36, 10623 Berlin, Germany

² Institute of Complex Systems (ICS-5: Molecular Biophysics),
Forschungszentrum Jülich, 52428 Jülich, Germany

³ Helmholtz-Zentrum Berlin für Materialien und Energie,
Hahn-Meitner-Platz 1, 14109 Berlin, Germany

⁴ Research-Educational Centre Bionanophysics, Moscow Institute of Physics
and Technology, 141700 Dolgoprudniy, Russia

E-mail: erik.guehrs@tu-berlin.de

New Journal of Physics **14** (2012) 013022 (7pp)


Received 30 September 2011

Published 13 January 2012

Online at <http://www.njp.org/>

doi:10.1088/1367-2630/14/1/013022

Abstract. We demonstrate an x-ray imaging method that combines Fourier transform holography with tomography ('tomoholography') for three-dimensional (3D) microscopic imaging. A 3D image of a diatom shell with a spatial resolution of 140 nm is presented. The experiment is realized by using a small gold sphere as the reference wave source for holographic imaging. This setup allows us to rotate the sample and to collect a number of 2D projections for tomography.

 Online supplementary data available from stacks.iop.org/NJP/14/013022/mmedia

⁵ Author to whom any correspondence should be addressed.

Contents

1. Introduction	2
2. Methods	3
3. Results and discussion	4
4. Summary	6
Acknowledgment	6
References	6

1. Introduction

The determination of the three-dimensional (3D) structure of samples is of much interest in various scientific areas. It can give insights into physical, chemical and biological processes and their functionality. Soft x-rays produced at synchrotron radiation sources are a versatile tomographic probe for micron-sized samples because they allow for sub- μm resolution imaging and have a penetration depth of the order of $1\ \mu\text{m}$, and because the tunability of the photon energy provides chemical sensitivity. As most objects show sufficient contrast using soft x-rays, it is not necessary to use staining procedures. High-resolution x-ray imaging has a broad range of applications in biology and physics. For example, it is widely used to determine the organization and function of inner-cell compartments and image magnetic processes in solid-state physics [1–4].

The recording of a 3D tomogram requires rotation of the sample to collect a dataset of 2D projections under different angles. The projections are assembled to a 3D image of the object using an inverse Radon transformation. In the soft x-ray regime, two methods have been commonly used in 3D imaging: x-ray transmission microscopy and, more recently, x-ray diffraction microscopy. The first approach uses Fresnel zone plates to focus the light scattered by the sample [5, 6], and a change in the optical setup allows a range of contrast mechanisms to be utilized, for example, bright-field contrast, Zernicke phase contrast or differential interference contrast [7, 8]. In contrast, x-ray diffraction microscopy works with a lensless setup recording the coherent diffraction pattern of a sample instead of a real-space image. The image is reconstructed using iterative algorithms together with *a priori* information such as the confinement of the sample to a finite area [9, 10]. In contrast to x-ray microscopy, no aberrations from optical elements are present. On the other hand, convergence of the phase retrieval algorithm to the true solution is not guaranteed in all cases.

Our objective is to demonstrate the feasibility of using tomoholography to obtain a 3D tomographic image reconstruction on the basis of 2D projections gained by Fourier transform holography (FTH). In principle, holography can be used to obtain 3D information on a sample from a single view. But the weak coherent scattering at large angles in the x-ray regimes makes it difficult to realize a high numerical aperture (NA) and a corresponding small depth-of-field [11].

FTH is a well-established imaging method allowing for an unambiguous solution of the phase problem via interference with a reference wave. Applications of FTH in the soft x-ray regime have been demonstrated, in particular for 2D imaging of magnetic as well as biological samples [3, 4, 12–16]. Similar to x-ray diffraction microscopy, a coherent diffraction pattern of the object is collected in the far-field region. The hologram is formed by the interference of the object wave with a known reference wave, which encodes the phase information as

modulation of the intensity. Hence, the phase problem can be solved non-iteratively by a single Fourier transform of the hologram, which yields the unambiguous reconstruction of the object exit wave. Usually an FTH geometry in the soft x-ray regime is realized using a transparent support membrane covered with an approximatively $1\ \mu\text{m}$ thick gold film acting as an opaque mask. An object aperture where the sample is deposited and a small pinhole (reference hole), which creates the reference wave, are fabricated by removing the gold film at these positions. As the reconstruction is formed by the convolution of the object exit wave with the reference exit wave, the size of the reference wave source, i.e. of the pinhole, limits the achievable spatial resolution [3, 17]. In FTH only simple optical elements are needed, avoiding any lens aberrations. Additionally, holography records the complex exit wave of the object; therefore it can be used *a posteriori* to calculate several contrast mechanisms used in microscopy (e.g. Zernicke phase contrast and differential interference contrast) [13].

With mask-based FTH it is not possible to rotate the sample to collect various angular positions for a tomographic dataset as the reference pinhole transmission is blocked at small angles due to the high aspect ratio of the reference hole, which is typically of the order of 1:10. Conic reference holes can increase the accessible rotation angle but may lead to an increased effective reference size due to x-ray transmission around the hole apex.

Due to Babinet's principle, a transparent membrane can be used instead of an opaque holographic mask. On this membrane the object as well as a point-like scatterer are placed and the interference between both structures forms the hologram [18]. The setup allows the rotation of the sample without blocking the reference wave and without deteriorating the resolution. As the test object we image a single shell of a diatom using a small gold sphere as the reference wave source. Diatoms are algae that are commonly found all over the world in sea water as well as fresh water. The complex structure of their shell and its biomineralization are of interest for biomimetic approaches in nanotechnology. Here, the intricate diatom shell serves as the test object for our proof-of-principle experiment.

2. Methods

The FTH geometry is sketched in figure 1: a single diatomic shell is prepared in the center of a transparent silicon nitride membrane ($1 \times 1\ \text{mm}^2$) carried by a silicon wafer. A gold sphere with a diameter of $250\ \text{nm}$ is placed close to the sample (distance $20\ \mu\text{m}$). During preparation a micromanipulator moves the diatom and gold sphere to the correct positions. The experiment is performed at the BESSY II U41-PGM beamline with a wavelength of $\lambda = 2.53\ \text{nm}$ at a wavelength resolution of $\frac{\lambda}{\Delta\lambda} \approx 3000$. The size of the x-ray probe is defined by a $39.5\ \mu\text{m}$ diameter pinhole placed $66\ \text{cm}$ upstream of the sample. The pinhole produces an Airy disc of $\sim 100\ \mu\text{m}$ at the sample position and is chosen such that the illumination function over the diatom and the gold reference is almost flat. Two guard pinholes remove the higher order diffraction of the primary pinhole. The monochromatized and spatially filtered x-ray beam provides sufficient lateral and longitudinal coherence to record holograms with high-contrast modulations. The sample is mounted on an $xyz\varphi$ -manipulator and the distance of the last guard pinhole from the sample allows for a rotation of the specimen orthogonal to the beam axis. As FTH reconstruction generates a focused image in the reference-source plane perpendicular to the x-ray beam, the sample is mounted such that the object-reference axis is collinear to the rotational axis [19]. This keeps the sample in the reference plane for all angular positions.

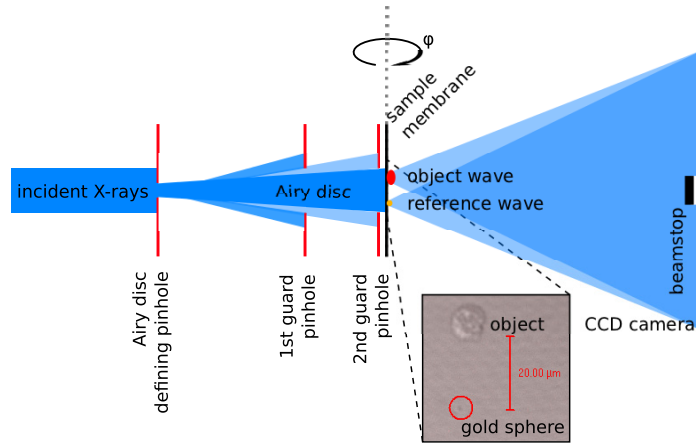


Figure 1. Scheme of the experiment setup. The sample on a rotation stage is coherently illuminated by an Airy disc which is produced by a pinhole placed upstream. Higher-order diffraction from the first pinhole is blocked using two guard pinholes between the primary pinhole and the sample. A charged coupled device (CCD) camera detects the hologram. The inset shows a light micrograph of the sample and the gold sphere.

The holograms are recorded using a charged coupled device (CCD) camera (Princeton Instruments PI-MTE, 2048×2048 pixels, pixel size $13.5 \mu\text{m}$) which is located 79 cm downstream of the sample. The distance between the sample and CCD camera is chosen such that the camera can sample the shortest-period modulations in the hologram, generated by the interference of the waves emerging from the object and the gold sphere. The corresponding depth-of-field ($d = \frac{\lambda}{2\text{NA}^2} = 4.1 \mu\text{m}$) exceeds the projected height of our object and is hence fulfilling the projection condition. A beamstop blocks the central part of the hologram in order to use the limited dynamic range of the CCD for high-momentum-transfer information.

3. Results and discussion

In total, 47 holograms are recorded from $\varphi = -60^\circ$ to $+55^\circ$ in 2.5° steps, with 0° referring to normal incidence. The exposure time of each hologram ranges 80 s to 400 s depending on the angular position and incident photon flux. The maximum tilt angles are limited by the size of the silicon nitride membrane, and the illuminating Airy disc, as higher angular positions result in strong diffraction from the silicon wafer facets surrounding the membrane which deteriorates the hologram. Before image reconstruction, an inverse Gaussian filter is applied to the hologram in order to suppress reconstruction artifacts from the sharp edges of the beamstop shadow. Additionally, the hologram is zeropadded, resulting in $36 \times 36 \text{ nm}^2$ pixel size in the projection images and $36 \times 36 \times 36 \text{ nm}^3$ voxel size in the 3D reconstruction. In figure 2 we show a representative hologram of the sample and the corresponding 2D reconstruction of the diatom at 0° tilt angle. The object–reference modulations are clearly visible, indicating sufficient coherence and adequate sampling even for high scattering vectors.

The resulting reconstructions have a lateral resolution of 130 nm (Rayleigh criterion) which is limited by the size of the gold sphere. The diatom appears as a bright object on a dark background although the object is absorbing x-rays more strongly than the nearly transparent

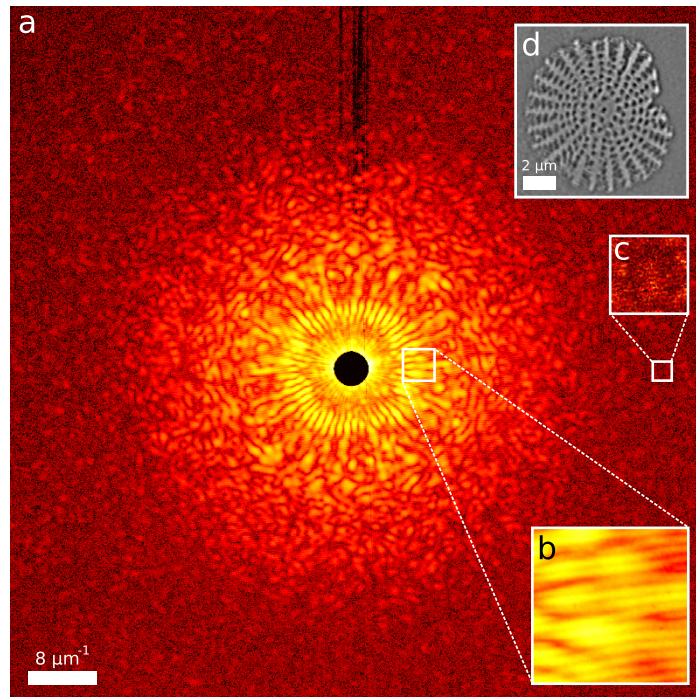


Figure 2. (a) Hologram (logarithmic intensity) of the sample at an angular position of 0° . The modulation between the object and reference waves is clearly visible in the insets (b) and (c) even for high scattering vectors, indicating sufficient coherence. The real-space reconstruction (d) of the hologram has a lateral resolution of 130 nm.

silicon nitride membrane. The reason for this contrast inversion is found in the absorptive character of the reference object.

On the basis of all 47 projections of the diatom the IMOD software package is applied for tomographic image reconstruction and for visualization [20]. The pores of the shell are used to determine the exact angular position and the axis of rotation of each projection. The additional introduction of fiducial markers into the sample is not necessary. The tomogram is calculated by weighted filtered back-projection. In figure 3, we present two slices of the tomographic back-projection of the diatom and a 3D rendered model of the surface. The shell of the diatom has a height of $1.3 \mu\text{m}$ and a diameter of $9.5 \mu\text{m}$. It is shaped rather like a soup bowl than a flat disc, which cannot be visualized by a single 2D projection. The shape is typical of diatoms of the genus *Stephanodiscus* and *Cyclotella*. The resolution of the tomogram was determined to be 140 nm by using Fourier shell correlation [21]. Movies showing virtual slices through the tomogram and a surface rendering of the diatom can be found in the supplementary material (online supplementary data available from stacks.iop.org/NJP/14/013022/mmedia).

Previous attempts at tomographic holography have applied either massive reference structures [22] or an in-line geometry [23]. But it is our approach of using a point-like scatterer in rigid FTH geometry that combines the stability, simplicity and flexibility of holographic imaging with a spatial resolution that is common in the established tomographic x-ray imaging methods. The approach can be used to image a large variety of objects as long as they can be placed on a support membrane. Higher spatial resolution can be achieved in future by the arrangement of one or more smaller gold spheres or by growing small platinum dots,

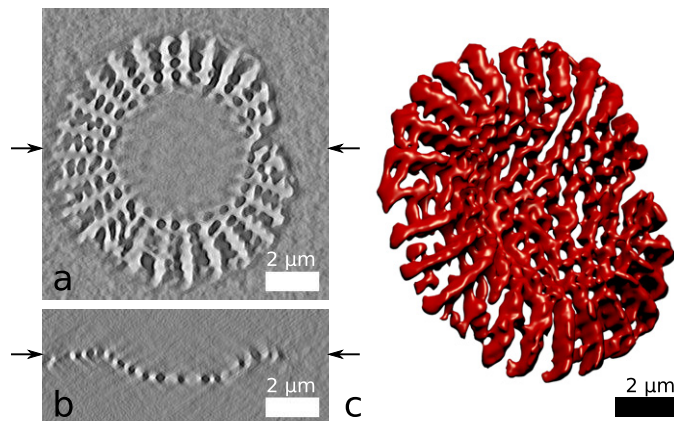


Figure 3. Two slices from the tomogram of the diatom: (a) top view and (b) side view. The resolution of the tomogram was determined to be 140 nm by using Fourier shell correlation. On the basis of the tomographic reconstruction, a 3D model of the shell was rendered (c). The arrows at each view indicate the position of the respective other slice.

e.g. by using focused ion beam technology. We expect that both types of reference structures can push the resolution below 50 nm if the incoming coherent photon flux is high enough to collect data at correspondingly high scattering vectors (as is already the case for the dataset presented here; see the inset of figure 2). We note that the approach can also be adapted for experiments on biomolecules at free-electron lasers (FEL). A small gold sphere could be connected to e.g. a protein complex via a DNA strand using biochemical linkers. This complex could be injected into the FEL beam by using a droplet source [24]. The holograms recorded at random projection directions would be assembled with approaches similar to those currently under development for coherent diffraction imaging [25].

4. Summary

We demonstrate the possibility of using a small reference scatterer in order to perform x-ray tomoholography. On the basis of 47 2D projections, we are able to reconstruct a 3D model of a diatomic shell with a spatial resolution of 140 nm. We anticipate that sub-50-nm resolution is achievable using smaller reference structures. Future high-resolution experiments may employ biochemically linked object–reference structures instead of arrangements on a support membrane.

Acknowledgment

We thank Peter Guttman from the Helmholtz–Zentrum Berlin for providing us with the diatoms.

References

- [1] Zschech E, Yun W and Schneider G 2008 High-resolution x-ray imaging—a powerful nondestructive technique for applications in semiconductor industry *Appl. Phys. A* **92** 423–9
- [2] Larabell C A and Le Gros M A 2004 X-ray tomography generates 3-D reconstructions of the yeast, *Saccharomyces cerevisiae*, at 60-nm resolution *Mol. Biol. Cell* **15** 957–62

- [3] Eisebitt S, Lörger M, Eberhardt W, Lüning J, Andrews S and Stöhr J 2004 Scalable approach for lensless imaging at x-ray wavelengths *Appl. Phys. Lett.* **84** 3373–5
- [4] Günther C M *et al* 2010 Microscopic reversal behavior of magnetically capped nanospheres *Phys. Rev. B: Condens. Matter* **81** 64411
- [5] Schmahl G, Rudolph D, Niemann B and Christ O 1980 Zone-plate x-ray microscopy *Q. Rev. Biophys.* **13** 297–315
- [6] Schneider G, Guttman P, Heim S, Rehbein S, Mueller F, Nagashima K, Heymann J B, Müller W G and McNally J G 2010 Three-dimensional cellular ultrastructure resolved by x-ray microscopy *Nat. Methods* **7** 985–7
- [7] Wilhein T, Kaulich B, Di Fabrizio E, Romanato F, Cabrini S and Susini J 2001 Differential interference contrast x-ray microscopy with submicron resolution *Appl. Phys. Lett.* **78** 2082–4
- [8] Rudolph G and Schmahl D 1987 *X-Ray Microscopy Instrumentation and Biological Applications* (Berlin: Springer)
- [9] Miao J, Charalambous P, Kirz J and Sayre D 1999 Extending the methodology of x-ray crystallography to allow imaging of micrometre-sized non-crystalline specimens *Nature* **400** 342–4
- [10] Shapiro D *et al* 2005 Biological imaging by soft x-ray diffraction microscopy *Proc. Natl Acad. Sci. USA* **102** 15343–6
- [11] McNulty I 1994 The future of x-ray holography *Nucl. Instrum. Methods Phys. Res. A* **347** 170–6
- [12] McNulty I, Kirz J, Jacobsen C, Anderson E H, Howells M R and Kern D P 1992 High-resolution imaging by Fourier transform x-ray holography *Science* **256** 1009–12
- [13] Guehrs E, Günther C M, Könecke R, Pfau B and Eisebitt S 2009 Holographic soft x-ray omni-microscopy of biological specimens *Opt. Express* **17** 6710–20
- [14] Pfau B *et al* 2011 Origin of magnetic switching field distribution in bit patterned media based on pre-patterned substrates *Appl. Phys. Lett.* **99** 062502
- [15] Stickler D *et al* 2010 Soft x-ray holographic microscopy *Appl. Phys. Lett.* **96** 042501
- [16] Scherz A *et al* 2007 Phase imaging of magnetic nanostructures using resonant soft x-ray holography *Phys. Rev. B* **76** 214410
- [17] Schlotter W F *et al* 2006 Multiple reference Fourier transform holography with soft x-rays *Appl. Phys. Lett.* **89** 163112
- [18] Stadler L-M, Gutt C, Autenrieth T, Leupold O, Rehbein S, Chushkin Y and Grübel G 2008 Hard x-ray holographic diffraction imaging *Phys. Rev. Lett.* **100** 245503
- [19] Guehrs E, Günther C M, Pfau B, Rander T, Schaffert S, Schlotter W F and Eisebitt S 2010 Wavefield back-propagation in high-resolution x-ray holography with a movable field of view *Opt. Express* **18** 18922–31
- [20] Kremer J R, Mastrorade D N and McIntosh J R 1996 Computer visualization of three-dimensional image data using IMOD *J. Struct. Biol.* **116** 71–6
- [21] van Heel M and Schatz M 2005 Fourier shell correlation threshold criteria *J. Struct. Biol.* **151** 250–62
- [22] McNulty I, Trebes J E, Brase J M, Yorkey T J, Levesque R, Szoke H, Anderson E H, Jacobsen C J and Kern D P 1993 Experimental demonstration of high-resolution three-dimensional x-ray holography *Proc. SPIE* **1741** 78–84
- [23] Watanabe N and Aoki S 1998 Three-dimensional tomography using a soft x-ray holographic microscope and CCD camera *J. Synchrotron Radiat.* **5** 1088–9
- [24] DePonte D P, Weierstall U, Schmidt K, Warner J, Starodub D, Spence J C H and Doak R B 2008 Gas dynamic virtual nozzle for generation of microscopic droplet streams *J. Phys. D: Appl. Phys.* **41** 195505
- [25] Hultdt G, Szoke A and Hajdu J 2003 Diffraction imaging of single particles and biomolecules *J. Struct. Biol.* **144** 219–27